Int. J. Heat Mass Transfer. Vol. 35, No. 5, pp. 1143–1154, 1992
Printed in Great Britain

0017–9310/92 $5.00 + 0.00

A fully implicit method for diffusion-controlled solidification of binary alloys

CHARN-JUNG KIM and MASSOUD KAVIANY
Department of Mechanical Engineering and Applied Mechanics, The University of Michigan, Ann Arbor, MI 48109, U.S.A.

(*Received* 1 *March* 1990 *and in final form* 3 *May* 1991)

Abstract—A recently developed numerical method for single-component phase-change problems is extended to treat some existing multi-domain models for diffusion-controlled solidification of binary alloys. The multi-domain models invoke a special difficulty associated with the unknown interface location and phase-transition temperature. Such a difficulty is efficiently resolved here by defining corrections similar to those used in single-phase convection problems. The field equations and the interfacial conditions are treated fully implicitly through the correction equations that are developed from the conservation of the interfacial fluxes. In addition, when a high disparity occurs between thermal and solutal mass diffusivities, renormalization of the length scales is suggested to improve spatial resolution of both the temperature and concentration fields. As a verification, several diffusion models that allow for analytical solutions are considered. Numerical solutions agree well with the available analytical solutions. The widely used assumption of a constant latent heat is found to be thermodynamically inconsistent under certain conditions and is clarified and corrected. A unique iteration procedure suggested in this study proves to be remarkably efficient and leads to fast convergence.

1. INTRODUCTION

THE PRESENT study is an extension of our previous works [1, 2] in which the use of conservative transformed equations was suggested in treating the single-component phase-change problems. Here, we consider the numerical solution to a class of diffusion-controlled solidification of binary alloys.

During solidification of binary systems, the solid–liquid interface exhibits a variety of microscopically complicated growth structures. There is also present a region in which both the solid and liquid phases coexist, which is often called the *mushy zone*. A comprehensive coverage of the solidification of binary mixtures is given in ref. [3]. A recent review of the various treatments in modeling of the mushy zone and their current status is provided in ref. [4]. Among a vast number of existing mathematical models for alloy solidification, we focus on some specific models based on the assumptions of macroscopically planar interfaces, local thermodynamic equilibrium, and the transport of heat and/or solute mass by diffusion alone. For convenience, these models are classified into four groups, which are briefly described below.

Model I assumes the existence of a single interface that distinctly separates both pure solid and pure liquid phases. The diffusion equations for the transport of heat and solute mass are written for individual phases, and their solutions are coupled through the interfacial conditions. Some analytical solutions exist in one-dimensional geometry [5–9]. Also, some semi-analytical and numerical solutions are available in the literature [10–13]. However, depending on the magnitude of the parameters, solutions to Model I may exhibit an arbitrary mushy zone in the liquid phase [14]. In Model II, the mushy zone is taken into consideration by assuming that its growth is controlled by heat diffusion; thus solidification occurs in an a priori known range of temperatures between solidus and liquidus temperatures. The local solid fraction in the mushy phase is assumed to vary linearly with either distance or temperature. Also, fixed values of effective heat capacity and thermal conductivity are used in the mushy zone, and several closed-form solutions are available [15–17]. Model III is the same as Model II except that the thermophysical properties of the mushy phase are weighted with respect to the local solid fraction, which is determined from the equilibrium phase diagram. Analytical solutions combined with numerical solutions can be found for semi-infinite media [18, 19]. Model IV is an extension of Model III and includes the solute mass diffusion. Therefore, the temperature and concentration fields are fully coupled through the interfacial conditions [20, 21]. This classification of existing models is made only for ease of presentation of the numerical method; for example, the distinction between Models II and III is made due to the different treatment of the mushy zone.

In this study, the numerical solution to Models I–III (excluding Model IV) are formulated by using a multi-domain approach. A unique feature of the multi-domain approach is the requirement for the imposition of the appropriate interfacial conditions. Generally, the temperature is assumed to be continuous at the interface, i.e. local thermodynamic equilibrium is assumed. In addition, two thermodynamic relations are specified at the interface; one is the equilibrium

NOMENCLATURE

A, A_m functions in finite-difference equations
a_i modified influence coefficients
C_i solute concentration field
c_i specific heat [J kg^{-1} K^{-1}]
c_r ratio of c_S/c_L
D_i solute mass diffusivity [m^2 s^{-1}]
d_i diffusion conductance
F_i total mass flux
f solid fraction in the mushy phase
$\hat{f}_1$ solid fraction at solid–mushy interface
G, H functions defined in equation (24)
Δh latent heat [J kg^{-1}]
Δh^* reference latent heat at T^* [J kg^{-1}]
h_i specific enthalpy [J kg^{-1}]
h_i^* reference enthalpy [J kg^{-1}]
i phase index or boundary index
J_i total flux of ϕ_i
$[\![\hat{J}]\!]_i$ ϕ-flux discontinuity at interface i
K partition coefficient, m_L/m_S
k_i thermal conductivity [W m^{-1} K^{-1}]
l^* reference length [m]
M_i total number of grid points within phase i
m_i coefficients for liquidus and solidus curves [K]
N total number of phases, Fig. 1
n geometry index
P Peclet number
p_i, q_i coefficients in correction equation (17)
Q heat sink [W m^{-1}]
Ste Stefan number, $\Delta h^*/(c_S T^*)$
T_i temperature field [K]
T^* reference temperature [K]
T_F freezing temperature of pure solvent [K]
$\hat{T}_i$ temperature at the interface i [K]
t time [s]
Δt time increment [s]
u_i velocity [m s^{-1}]
V_i variable, $x^{n+1}/(n+1)$
$\hat{v}_i$ variable defined in equation (15)
x spatial coordinate [m]
$\hat{x}_i$ position of interface i [m].

Greek symbols
α_i thermal diffusivity [m^2 s^{-1}]
α^* reference thermal diffusivity of the mushy phase [m^2 s^{-1}]
β_i dimensionless number
Γ_i effective diffusion coefficient
γ_i variable in correction equation
δ_C solutal boundary-layer thickness [m]
δ_S solid-phase thickness [m]
δ_i thickness of phase i [m]
ε convergence criterion, equation (18)
η similarity variable
θ_i ($\hat{\theta}_i$) dimensionless temperature, T_i/T^* ($\hat{T}_i/T^*$)
λ similarity constant or dimensionless solid-phase thickness
λ_C dimensionless thickness of solutal boundary layer
λ_h dimensionless thickness of thermal boundary layer
μ_{iA} (μ_{iB}) variable, $\partial\hat{\phi}_{iA}/\partial\hat{T}_i$ ($\partial\hat{\phi}_{iB}/\partial\hat{T}_i$)
ξ_i transformed coordinate for phase i
ρ_i density [kg m^{-3}]
ρ_r ratio of ρ_S/ρ_L
σ parameter, equation (30)
τ dimensionless time
ϕ general dependent variable
$\bar{\phi}$ $(\hat{\phi}+\phi)/2$
ψ h_S-h
ω_i' dimensionless number for position correction.

Superscripts
N corrected value
$*$ reference
$\wedge$ interface
$'$ correction term.

Subscripts
i, $i+1$ phase or boundary indices
iA (iB) ahead (backward) of interface i
L liquid
S solid.

Other symbols
$[\![\varphi]\!]_i$ $\varphi_{iA}-\varphi_{iB}$ for any quantity φ
$|\varphi|$ absolute value of φ.

phase diagram [3], and the other is the enthalpy–temperature relation which leads to the definition of the latent heat [22]. The concentration discontinuity at the interface is dependent on the interface temperature (from an equilibrium phase diagram), as is the enthalpy discontinuity at the interface (from enthalpy–temperature relations). When the assumed constant specific heats are different between phases, this enthalpy discontinuity at the interface (i.e. latent heat) varies with the interface temperature. However, we observe that this variable latent heat has been unrecognized in a large number of previous works. Under these circumstances, the use of constant latent heat leads to a thermodynamic inconsistency and, as a result, violates the overall conservation of energy. (Only when the variation in the latent heat is negligible, can the overall energy conservation be satisfied within an acceptable range.) Therefore, the validity of

the use of a constant latent heat should be examined for case application. We will examine the consequence of the use of the thermodynamically inconsistent assumption in connection with our formulation of numerical solutions. It is interesting to note that in contrast to the existing temperature-based formulations, in which the constant latent heat has been liberally used, the variable latent heat has been correctly implemented in enthalpy-based formulations such as in refs. [23–25].

The major difficulties with multi-domain approaches are associated with unknown interface location and/or interface temperature (these can even be time dependent). Determination of these unknowns requires the simultaneous solution of individual field equations that match the interfacial conditions; thus the problem is highly nonlinear. As a result, the capability of accurately tracking the interface location and/or accurately predicting the interface temperature is crucial in developing a numerical method. Here, we propose a fully implicit method that overcomes these difficulties by using a successive iteration. A novel iteration scheme is developed that is analogous to the SIMPLE algorithm [26] using the pressure-correction equation to solve the momentum equations. For this, we introduce a general temperature- and position-correction equation that improves the intermediate solutions during iterations. The correction equations are derived from the continuity conditions of the interfacial fluxes and are solved simultaneously to update the interface temperature and position. This unique solution procedure proves to be efficient and allows for rapid convergence. The present numerical method is applicable to both unbounded- and finite-domain problems and is able to account for a general phase diagram. Furthermore, in the case of Model I, the existence of steep concentration gradients near the interface is found to be easily handled by renormalizing the length scales in the liquid phase using the thermal and solutal boundary-layer thicknesses. This allows for a more efficient computation compared with the bilinear mapping [12] and the use of a large number of grid points [9]. The performance of the present numerical method is tested against a few example problems. Even without any modification, the present numerical method is applicable to some practical problems, such as the modeling of the microsegregation in binary metallic alloys [27].

2. NUMERICAL FORMULATION

In this section, we describe the numerical method applicable to Models I and II. The treatment of Model III requires minor modifications, which will be discussed later. Figure 1 illustrates a multi-domain system for which an index i is assigned to each phase and $\hat{x}_i$ stands for the right boundary of phase i. The density of phase i is assumed to be constant, and its specific enthalpy h_i is defined as

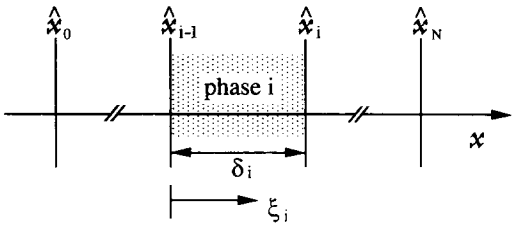

FIG. 1. A multi-domain system composed of N distinguishable phases. A representative phase is highlighted.

$$h_i = \int_{T^*}^{T_i} c_i \, \mathrm{d}T + h_i^* \tag{1}$$

where h_i^* is the reference enthalpy at a reference temperature T^*. Unless otherwise specified, $h_i^* = 0$ will be used for a pure solid phase and $h_i^* = \Delta h^*$ for a pure liquid phase, where Δh^* stands for a *reference latent heat* at T^*. For the sake of brevity, we use a general dependent variable ϕ to denote either a specific enthalpy h or a solute concentration C (when ϕ stands for the mixture mass, $\phi = 1$ will be used). Then, the governing equation for ϕ_i is

$$\frac{\partial}{\partial t}(x^n \rho_i \phi_i) + \frac{\partial}{\partial x}\left(x^n \rho_i u_i \phi_i - x^n \Gamma_i \frac{\partial \phi_i}{\partial x}\right) = 0 \tag{2}$$

where n is the geometry index, $\Gamma_i = \rho_i \alpha_i$ for $\phi_i = h_i$, and $\Gamma_i = \rho_i D_i$ for $\phi_i = C_i$. The moving boundaries are immobilized by introducing a coordinate transformation $x = x(\xi_i, t)$. The above equation is then transformed into [1]

$$\frac{\partial}{\partial t}\left(\rho_i \phi_i \frac{\partial V_i}{\partial \xi_i}\right) + \frac{\partial J_i}{\partial \xi_i} = 0 \tag{3}$$

with

$$V_i = \frac{1}{n+1} x^{n+1}$$

$$J_i = F_i \phi_i - \frac{x^n \Gamma_i}{(\partial x/\partial \xi_i)} \frac{\partial \phi_i}{\partial \xi_i}$$

$$F_i = \rho_i \left(x^n u_i - \frac{\partial V_i}{\partial t}\right) \tag{4}$$

where F_i is the total flux of mixture mass and J_i is that of ϕ_i. The immobilization of the moving boundaries creates the pseudo-convection in the transformed coordinate [28] so that F_i can have a non-zero value even in the absence of the velocity field.

Now, suppose that phase transition is occurring across an interface i. At this interface, the temperature is continuous from the assumption of thermodynamic equilibrium, and the interfacial fluxes are continuous from the conservation principles, i.e.

$$T_i = T_{i+1}, \quad F_i = F_{i+1}, \quad J_i = J_{i+1} \tag{5}$$

where all the quantities are evaluated at the interface $\hat{x}_i$. In addition, the values of ϕ_i and ϕ_{i+1} at the inter-

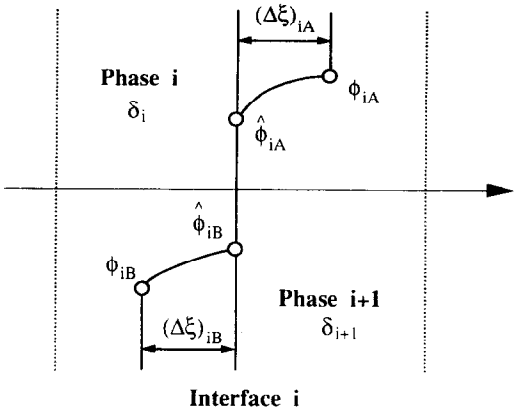

FIG. 2. Finite-volume elements adjacent to the phase interface i.

face are determined from the given thermodynamic relations (equilibrium phase diagram for $\phi = C$ and enthalpy–temperature relations for $\phi = h$). When the values of $\hat{x}_i$ and $\hat{T}_i$ are known, numerical solutions of equation (3) are easily obtained as described in ref. [1]. Therefore, only the special features arising from the determination of $\hat{x}_i$ and $\hat{T}_i$ will be presented below.

For convenience, subscripts iA and iB indicate *ahead* and *backward* of the interface i, respectively. Therefore, whenever ϕ varies discontinuously across the interface i, each value of ϕ at the interface will be designated by $\hat{\phi}_{iA}$ and $\hat{\phi}_{iB}$, respectively, as shown in Fig. 2. Next, we use the linear transformation

$$x = \delta_i \xi_i + \hat{x}_{i-1}, \quad \delta_i = \hat{x}_i - \hat{x}_{i-1} \tag{6}$$

where $0 \leqslant \xi_i \leqslant 1$ and δ_i is the thickness of phase i. For efficient computations in treating Model I, $\hat{x}_i$ is allowed to take different values for the enthalpy and concentration fields. This is because a high disparity between thermal and solutal diffusivities causes the corresponding boundary-layer thicknesses in the liquid phase to be substantially different. For the finite control-volumes adjacent to the interface i, shown in Fig. 2, the interfacial ϕ-fluxes are expressed as

$$\begin{aligned} \hat{J}_{iA} &= \hat{F}_i \bar{\phi}_{iA} + a_{iA}(\hat{\phi}_{iA} - \phi_{iA}) \\ \hat{J}_{iB} &= \hat{F}_i \bar{\phi}_{iB} + a_{iB}(\phi_{iB} - \hat{\phi}_{iB}) \end{aligned} \tag{7}$$

with

$$\begin{aligned} a_{iA} &= d_{iA} A_m(\hat{F}_i/d_{iA}), \quad a_{iB} = d_{iB} A_m(\hat{F}_i/d_{iB}) \\ d_{iA} &= \frac{\hat{x}_i'' \hat{\Gamma}_{iA}}{\delta_{i+1}(\Delta\xi)_{iA}}, \quad d_{iB} = \frac{\hat{x}_i'' \hat{\Gamma}_{iB}}{\delta_i (\Delta\xi)_{iB}} \\ \bar{\phi}_{iA} &= \frac{\hat{\phi}_{iA} + \phi_{iA}}{2}, \quad \bar{\phi}_{iB} = \frac{\hat{\phi}_{iB} + \phi_{iB}}{2} \end{aligned} \tag{8}$$

where $\hat{J}_{iA}$ is the total ϕ-flux entering phase $(i+1)$ and $\hat{J}_{iB}$ is that leaving phase i. We define the function $A_m(P)$ as

$$A_m(P) = A(P) + 0.5|P| \tag{9}$$

Table 1. Function $A(P)$ for different schemes (from ref. [26])

Scheme	Formula for $A(P)$
Central difference	$1-0.5\|P\|$
Upwind	1
Hybrid	$\max\{0, 1-0.5\|P\|\}$
Power law	$\max\{0, (1-0.1\|P\|)^5\}$

where $A(P)$ is selected from Table 1 for the desired scheme. The rationale for introducing this modified function $A_m(P)$ will be discussed in the next section. From equation (5), we have

$$[\![\hat{J}]\!]_i \equiv \hat{J}_{iA} - \hat{J}_{iB} = 0. \tag{10}$$

However, unless $\hat{x}_i$ and $\hat{T}_i$ are correctly specified, the resulting solution may not satisfy the above equation. Therefore, newly-guessed values of $\hat{x}_i$ and $\hat{T}_i$ should be found such that they result in smaller $[\![\hat{J}]\!]_i$. These iterations continue until equation (10) is satisfied within a prescribed tolerance. One simple way to improve the tentative values of $\hat{x}_i$ and $\hat{T}_i$ is to begin by assuming that the correct values of $\hat{x}_i$ and $\hat{T}_i$ are obtained from

$$\hat{T}_i^N = \hat{T}_i + \hat{T}_i', \quad \hat{x}_i^N = \hat{x}_i(1+\omega_i') \tag{11}$$

where $\hat{T}_i'$ will be called the *temperature correction* and ω_i' the *position correction*. The correct value of $\hat{J}_{iA}$ is then expressed as

$$\begin{aligned} \hat{J}_{iA}^N = {} & (\hat{F}_i + \hat{F}_i')(\bar{\phi}_{iA} + \bar{\phi}_{iA}') \\ & + (a_{iA} + a_{iA}')(\hat{\phi}_{iA} - \phi_{iA} + \hat{\phi}_{iA}' - \phi_{iA}'). \end{aligned} \tag{12}$$

The new correction terms appearing in the above equation are to be determined by retaining only the first-order correction terms as follows. Expanding $\hat{\phi}_{iA}^N$ in terms of $\hat{T}_i'$ gives

$$\hat{\phi}_{iA}^N = \hat{\phi}_{iA} + \left(\frac{\partial \hat{\phi}_{iA}}{\partial \hat{T}_i}\right) \hat{T}_i' + \cdots$$

and defining $\mu_{iA} = (\partial \hat{\phi}_{iA}/\partial \hat{T}_i)$ yields

$$\hat{\phi}_{iA}' = \mu_{iA} \hat{T}_i'. \tag{13}$$

The correction term ϕ_{iA}' is assumed to depend only on $\hat{T}_i'$ and approximated as

$$\phi_{iA}' = (1-\gamma_{iA})\mu_{iA} \hat{T}_i' \tag{14}$$

where γ_{iA} is a constant chosen properly. A rigorous analysis for the determination of γ_{iA} is not attempted here, since, as will be shown, even a constant value of γ_{iA} leads to fast convergence. By combining equations (4) and (11) and by assuming no contribution from the velocity term, $\hat{F}_i'$ becomes

$$\hat{F}_i' = -\hat{v}_i \omega_i', \quad \hat{v}_i = \frac{\rho_i \hat{x}_i^{n+1}}{\Delta t}. \tag{15}$$

From $\delta_{i+1} = \hat{x}_{i+1} - \hat{x}_i$ and equation (11), we have

$$\delta_{i+1}' = \delta_{i+1} \omega_i' + \hat{x}_{i+1}(\omega_{i+1}' - \omega_i').$$

Then, a correct value of d_{iA}^N is expressed as

$$d_{iA}^N = d_{iA}(1+\omega_i')^n\left(1-\frac{\delta_{i+1}'}{\delta_{i+1}}\right)$$

or

$$\frac{d_{iA}'}{d_{iA}} = (n-1)\omega_i' + \frac{\hat{x}_{i+1}}{\delta_{i+1}}(\omega_i'-\omega_{i+1}'). \tag{16}$$

Next, for simplicity we assume $a_{iA}'/a_{iA} = d_{iA}'/d_{iA}$ by neglecting any change in the value of $A_m(\hat{F}_i/d_{iA})$. At this point, by using the correction terms derived so far, $\hat{J}_{iA}^N$ can be expressed in terms of $\hat{T}_i'$, ω_i' and ω_{i+1}'. If we treat $\hat{J}_{iB}^N$ in a way similar to the above and insert resulting expressions for $\hat{J}_{iA}^N$ and $\hat{J}_{iB}^N$ into equation (10), we obtain the following first-order correction equation:

$$p_i\omega_i' + q_i\hat{T}_i' + [\![\hat{J}]\!]_i = p_{iA}\omega_{i+1}' + p_{iB}\omega_{i-1}' \tag{17}$$

where

$$p_i = p_{iA} + p_{iB} + (n-1)[\![\hat{J}-\hat{F}\bar{\phi}]\!]_i - [\![\hat{v}\bar{\phi}]\!]_i$$

$$q_i = (a\mu\gamma)_{iA} + (a\mu\gamma)_{iB} + [\![(1-\gamma/2)\mu\hat{F}]\!]_i$$

$$p_{iA} = \frac{\hat{x}_{i+1}}{\delta_{i+1}}(\hat{J}-\hat{F}\bar{\phi})_{iA}, \quad p_{iB} = \frac{\hat{x}_{i-1}}{\delta_i}(\hat{J}-\hat{F}\bar{\phi})_{iB}.$$

The above correction equation (17) is found to be readily solvable since the number of correction equations is always equal to that of the unknowns. Due to the approximate nature of the correction equations, the use of an underrelaxation is helpful in obtaining converged solutions. Note that, if all the values of $[\![\hat{J}]\!]_i$ are zero, no corrections are required. Once the required correction terms are determined, the tentative values of $\hat{x}_i$ and $\hat{T}_i$ are updated from equation (11), but the interfacial $\hat{\phi}$-values are determined from the given thermodynamic relations. Iteration continues until the convergence criterion

$$\left|\frac{[\![\hat{J}]\!]_i}{|\hat{J}_{iA}|+|\hat{J}_{iB}|}\right| \leqslant \varepsilon \tag{18}$$

is satisfied, where ε is a prescribed tolerance. In the following test problems, after some trial runs, the value of ε is selected to be 0.001. An initial guess for $\hat{F}_i^N$ (thus $\hat{x}_i^N$) can be obtained explicitly from equation (7) as

$$\hat{F}_i^N = \hat{F}_i - \frac{[\![\hat{J}]\!]_i}{[\![\bar{\phi}]\!]_i} \tag{19}$$

which is identical to equation (18) in ref. [1]. In Model I, either $\phi = C$ or h can be used to evaluate $\hat{F}_i^N$ with the interface temperature fixed (i.e. $\hat{T}_i^N = \hat{T}_i$). Alternatively, the values of $\hat{F}_i$ and $\hat{T}_i$ at the previous time step can also be used as the initial guesses for $\hat{F}_i^N$ and $\hat{T}_i^N$ (note that equation (19) reduces to $\hat{F}_i^N = \hat{F}_i$ when $[\![\hat{J}]\!]_i = 0$).

The overall solution procedure presented above resembles that used for solving the momentum equations discussed in ref. [26]; for example, $[\![\hat{J}]\!]_i$ in the present study plays a role similar to the mass source in the SIMPLE algorithm.

3. TEST PROBLEMS

3.1. *Model I*

Consider first the solidification of a dilute binary alloy in a semi-infinite plane for which phases 1 and 2 are the pure solid and pure liquid phases, respectively. The thermophysical properties, except the latent heat, are assumed to be constant within each phase, but they may differ between phases. The treatment of the latent heat is based on the enthalpy–temperature relation given in equation (1). By linearizing the equilibrium phase diagram, the liquidus and solidus lines are given as

$$\hat{T}_1 = T_F - m_1\hat{C}_{1B} = T_F - m_2\hat{C}_{1A} \tag{20}$$

where T_F is the freezing temperature of a pure solvent. With the interface conditions discussed previously, the additional conditions are specified as

$$\text{at } t = 0: \quad C_2 = \hat{C}_2, \quad T_2 = \hat{T}_2, \quad \delta_1 = 0$$

$$\text{at } x = 0: \quad T_1 = \hat{T}_0, \quad \frac{\partial C_1}{\partial x} = 0$$

$$\text{at } x = \infty: \quad \frac{\partial T_2}{\partial x} = 0, \quad \frac{\partial C_2}{\partial x} = 0 \tag{21}$$

where $\hat{T}_0$, $\hat{T}_2$ ($\geqslant T_F - m_2\hat{C}_2$) and $\hat{C}_2$ are fixed values. The analytical solutions subject to the above conditions are reported in the work of Tsubaki and Boley [7] as an extension of Rubinstein's solution [6]. However, a constant latent heat is always used in their work; therefore, when $c_1 \neq c_2$, their interfacial energy balance becomes inconsistent with the enthalpy–temperature relations on which their temperature-field equations are based. Therefore, modified analytical solutions, which are thermodynamically consistent, are given below for the completeness. Using the enthalpy–temperature relation (1) at the interface and introducing a similarity variable $\eta = x(4D_2t)^{-1/2}$, the analytical solutions are

$$\delta_1(t) = 2\lambda\sqrt{(D_2t)}, \quad C_1 = K\hat{C}_{1A}$$

$$\frac{T_1-\hat{T}_0}{\hat{T}_1-\hat{T}_0} = \frac{\operatorname{erf}(\beta_1\eta)}{\operatorname{erf}(\beta_1\lambda)}$$

$$\frac{T_2-\hat{T}_2}{\hat{T}_1-\hat{T}_2} = \frac{\operatorname{erfc}\{\beta_2\eta+\beta_2\lambda(\rho_r-1)\}}{\operatorname{erfc}(\beta_2\lambda\rho_r)}$$

$$\frac{C_2-\hat{C}_2}{\hat{C}_{1A}-\hat{C}_2} = \frac{\operatorname{erfc}\{\eta+\lambda(\rho_r-1)\}}{\operatorname{erfc}(\lambda\rho_r)}$$

$$\rho_r = \frac{\rho_1}{\rho_2}, \quad K = \frac{m_2}{m_1}$$

$$\beta_1 = \sqrt{\left(\frac{D_2}{\alpha_1}\right)}, \quad \beta_2 = \sqrt{\left(\frac{D_2}{\alpha_2}\right)}. \tag{22}$$

Table 2. The parameters used in the computation and the corresponding analytical solutions from equation (23). Other parameters are fixed such that $\hat{C}_2 = 0.1$, $m_1/T_F = 0.6$, $m_2/T_F = 0.4$, $D_1/\alpha_1 = 1$ and $T^* = T_F$

Case	ρ_r	c_r	β_1	β_2	$\hat{\theta}_0$	$\hat{\theta}_2$	*Ste*	λ	λ_C	λ_h	$\hat{\theta}_1$
A	1.00	1/9	1/3	1.000	0.50	1.10	1.500	0.7924	1.3378	1.3378	0.9480
B	1.00	1.0	0.050	0.050	0.50	1.10	1.500	6.5949	0.3368	31.957	0.9403
C	0.92	0.4	0.024	0.082	0.95	1.07	0.654	0.5083	1.5134	21.876	0.9515

A similarity constant λ is obtained from the two transcendental equations

$$T^{**}(\lambda\rho_r)\left\{\frac{c_1}{G(\beta_1\lambda)}+\frac{c_2}{H(\beta_2\lambda\rho_r)}+c_1-c_2\right\}$$
$$=\frac{c_1(\hat{T}_0-T^*)}{G(\beta_1\lambda)}+\frac{c_2(\hat{T}_2-T^*)}{H(\beta_2\lambda\rho_r)}+\Delta h^*$$
$$\hat{T}_1-T^*\equiv T^{**}(\lambda\rho_r)=T_F-T^*-\frac{m_2\hat{C}_2}{1-(1-K)H(\lambda\rho_r)} \quad (23)$$

where

$$G(x)=\sqrt{\pi}x\exp(x^2)\operatorname{erf}(x),$$
$$H(x)=\sqrt{\pi}x\exp(x^2)\operatorname{erfc}(x). \quad (24)$$

For large values of x, an asymptotic expansion of $H(x)$ gives [29]

$$H(x)\cong 1+\sum_{j=1}^{\infty}\frac{1\cdot 3\cdots(2j-1)}{(-2x^2)^j}.$$

In the case of $c_1\neq c_2$, the above analytical solutions yield different results from those of Tsubaki and Boley [7] since a variable instead of constant latent heat has been incorporated into equation (23). The magnitude of a few sets of parameters and the corresponding analytical solutions from this study are listed in Table 2. The dimensionless temperature $\hat{\theta}_i$ and the dimensionless latent heat *Ste* are defined in the Nomenclature. Each value of λ_ϕ in Table 2 is evaluated from the analytical solution such that

$$\frac{\phi_2-\hat{\phi}_2}{\hat{\phi}_{1A}-\hat{\phi}_2}=0.01 \quad \text{at} \quad \eta=\lambda+\lambda_\phi. \quad (25)$$

Then, if a time-dependent length scale $2\sqrt{(D_2t)}$ is used (due to the lack of a physical length scale), λ_ϕ is interpreted as a dimensionless thickness of the corresponding boundary layer in the liquid phase and λ as a dimensionless thickness of the solid phase.

Numerical solutions are obtained by employing the power-law scheme and by using $M_1=M_2=20$, where M_i is the total number of grid points within phase i. The thickness of the solid phase, δ_1, is the same for both the temperature and concentration fields. As was mentioned, thermal and solutal boundary-layer thicknesses in the liquid phase may differ from each other depending on the value of β_2 (approximately of the order of λ_C/λ_h); therefore, each value of δ_2 is selected to be sufficiently larger than the corresponding boundary-layer thickness, while a ratio of δ_2/δ_1 for each ϕ-field is made to remain constant at all times. The initial profiles are obtained from the analytical solution by assuming that $\delta_1/l^*=10^{-5}$, and the calculation continues until $\delta_1/l^*=10^5$ (special care is required for start-up with arbitrarily specified profiles). For this problem, the correction equation (17) provides two linear equations for two unknowns ω_1' and $\hat{T}_1'$ (note that $\omega_0'=0$ and $\omega_2'=\omega_1'$). Numerical solutions for λ and $\hat{\theta}_1$ initially undergo transient periods up to $\delta_1/l^*\sim 8\times 10^{-5}$ and thereafter attain asymptotic values that agree to within 0.4% of the corresponding analytical solutions listed in Table 2. The converged solution at each time step is obtained within four iterations after the transient period. When the local temperature and concentration at grid points (in the ξ_i coordinate) are examined, an asymptotic behavior is observed. This is because the ξ_i coordinate is directly related to the similarity variable η; for example

$$\xi_1=\frac{\eta}{\lambda_n} \quad (26)$$

where λ_n is a numerically obtained similarity constant that is evaluated from $\lambda_n=\delta_1(4D_2t)^{-1/2}$ and is close to the exact value of λ. Since λ_n remains nearly constant, the transformed coordinate ξ_1 has a role of another similarity variable; thus the numerical solution of T_1 (or h_1) can be expressed approximately as

$$\frac{T_1-\hat{T}_0}{\hat{T}_1-\hat{T}_0}=\frac{\operatorname{erf}(\beta_1\lambda_n\xi_1)}{\operatorname{erf}(\beta_1\lambda_n)}. \quad (27)$$

Therefore, the transient temperature field in the ξ_1 coordinate remains isothermal at each grid point, which represents a feature similar to the isotherm migration methods [30, 31], although the treatment of the grid location and the corresponding node temperature is reversed. Note that if the above expression for T_1 is inserted into the transformed equation (3), a differential equation $\mathrm{d}\delta_1^2/\mathrm{d}t=4\lambda_n^2D_2$ is obtained as expected. A similar argument is also valid for the transformed coordinate ξ_2.

We now discuss the motivation for the choice of the function $A_m(P)$. First, the interfacial flux of solute mass into the liquid phase is considered below, but the following argument is valid for other interfacial fluxes. From equations (4) and (8), the corresponding Peclet number is

$$|P|=\frac{|\hat{F}_1|}{d_{1A}}\sim\frac{\rho_r(\Delta\xi)_{1A}}{D_2}\delta_C\frac{\mathrm{d}\delta_1}{\mathrm{d}t}$$

where δ_C stands for a solutal boundary-layer thickness. Since $\delta_C/\delta_1 \sim \lambda_C/\lambda$ and $\delta_1 = 2\lambda\sqrt{(D_2 t)}$, we have

$$|P| \sim 2\rho_r \lambda \lambda_C (\Delta\xi)_{1A} \tag{28}$$

which indicates that a low Peclet number is associated with the moving interface (e.g. see Table 2). It is evident that the function $A_m(P)$ is the most convenient form when the interfacial fluxes are central-differenced utilizing a low Peclet number behavior as explained above. Furthermore, even when the power-law scheme is preferred to ensure the physical reality of the solution [26], the use of $A_m(P)$ reduces the nonlinearity in $A(P)$ thus leads to fast convergence. (This is also valid for other schemes since the interface Peclet numbers are relatively low.)

We further discuss the possibility of the occurrence of thermodynamic inconsistency mentioned earlier. In order to clarify this point, we rewrite equation (5) for $\phi = h$ in a conventional form as

$$k_S \frac{\partial T_S}{\partial x} - k_L \frac{\partial T_L}{\partial x} = \rho_S \Delta h \frac{d\delta}{dt} \quad \text{at} \quad x = \delta(t)$$

$$\Delta h = h_L - h_S \quad \text{at} \quad T = \hat{T} \tag{29}$$

where subscripts i and $i+1$ are replaced by subscripts S and L, $\delta(t)$ is the location of the interface, and $\hat{T}$ the interface temperature. When the specific heats are constant, the latent heat Δh follows from equation (1) as

$$\Delta h = \Delta h^*(1+\sigma), \quad \sigma = \frac{(c_L - c_S)(\hat{T} - T^*)}{\Delta h^*} \tag{30}$$

where σ is introduced here to investigate the effects of the latent heat variation. Equation (23) shows that even for a given binary system the interface temperature varies, subject to the changes in the external parameters such as the wall temperature. Therefore, in the case of $c_S \neq c_L$, the use of a constant latent heat as in ref. [7] causes an ambiguity. The variable latent heat arising from the unequal specific heats between phases seems to have significant effects especially when σ changes with time (i.e. $c_S \neq c_L$ and time-dependent $\hat{T}$) as encountered in finite-domain problems [8–12].

As a first approximation, we use the magnitude of σ in equation (30) to estimate the degree of energy-conservation failure caused by the thermodynamic inconsistency. This is because if σ is negligibly small, the overall energy balance can be satisfied within an acceptable range. In order to find out the value of σ, two sample cases are selected; one is of the results of Fig. 6 in ref. [11] and the other is of those of Fig. 2 in ref. [9]. Based on the parameters used in ref. [11] (selecting $T^* = 272.65$ K and $\hat{T} = 251.95$ K), $|\sigma|_{max}$ is found to be ~ 0.17. For the second case, $|\sigma|_{max} \sim 0.28$ is observed. Compared with the claimed accuracies in their solutions, the estimated values of σ are relatively large.

For more quantitative comparisons, the present numerical method is applied to solve the inward solidification of a binary alloy confined in a sphere of radius l^*, which is treated in ref. [9]. (The details can be found there, but recall that the variable latent heat from the h–T relation is used in our study.) Numerical solutions are obtained as described previously but with some minor modifications. The parameters in Cases A and B of Table 2 are the same as those used for Figs. 2 and 8 shown in ref. [9], respectively. Computation is performed with $M_1 = 30$ and $M_2 = 20$. The overall energy and solute mass balances are satisfied to within 0.15% at each time step. The converged solutions are obtained to within ten iterations for both cases. The present numerical solutions for Case A show that the dimensionless time for the complete solidification is $\tau = 2.79$ where τ is the same as y defined in the work of Gupta [9]. However, in his numerical results the complete solidification was not attained even for $\tau = 3.28$, which is unphysical due to violation of conservation principles.† The present numerical results corresponding to Case B are shown in Fig. 3. The numerical results from ref. [9] are also shown for comparison. In particular, this study gives the following results at time $\tau = 0.195$.

- The thickness of the solid phase (say δ_S) is found to be $0.174l^*$, i.e. $\delta_S/(2\lambda\sqrt{(D_L t)}) = 1.09$ with the value of λ given in Table 2.

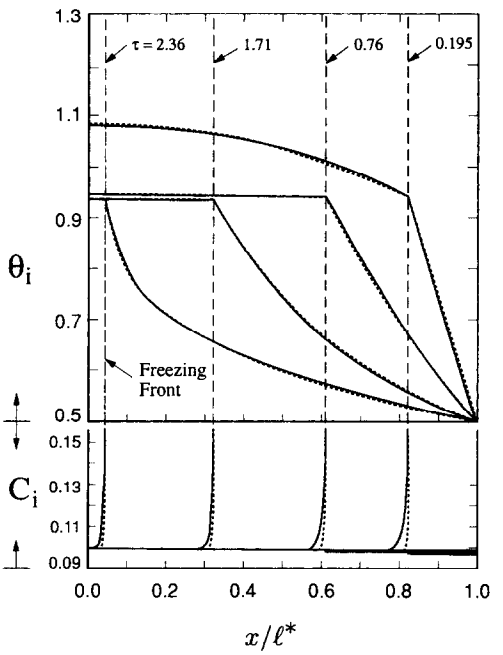

FIG. 3. Temperature and solute concentration profiles for various elapsed times: numerical results from ref. [9] (solid lines), and from this study (dotted lines). In the solid phase, the concentration profiles obtained from this work are not shown in the figure. A dimensionless time τ is the same as y defined in ref. [9].

† See Fig. 2 in ref. [9] and also note that no attempts have been made there to verify the overall energy balance.

● The solutal boundary-layer thickness in the liquid phase (say δ_C) is found to be $\delta_C = 0.04\delta_S$.

The corresponding concentration profile from ref. [9] clearly shows that $\delta_C/\delta_S > 0.15$ which is substantially greater than that from this study. Note that in the case of a planar geometry a value of δ_C/δ_S is the same as that of λ_C/λ, which is about 0.05 (from Table 2). Apart from the disagreement with the concentration profiles, the present numerical results shown in Fig. 3 agree well with those from ref. [9] mainly because of the condition $c_S = c_L$ used in Case B. However, when compared with the numerical studies in ref. [9], our numerical method allows for a substantial decrease in the number of grid points (up to an order of magnitude smaller). The results in Fig. 3 show that an artificial mushy zone exists in the vicinity of the interface and that this is consistent with the observation in ref. [14] mentioned earlier.

3.2. *Model II*

In this model, the growth of the mushy zone is controlled by heat diffusion [15–17] and solidification occurs in a range of temperatures between solidus and liquidus temperatures. We use indices 1–3 to designate the solid, mushy and liquid phases, respectively, and assume that the densities are equal between phases (i.e. $\rho_1 = \rho_2 = \rho_3$). The effect of solute concentration is considered only through a linear relation between the solid fraction f and the temperature in the mushy zone T_2, such that [17]

$$f = \hat{f}_1\left(1 - \frac{T_2 - \hat{T}_1}{\hat{T}_2 - \hat{T}_1}\right) \tag{31}$$

where $\hat{f}_1$ is a constant solid-fraction at the solidus front $\hat{x}_1$ and the fixed values of $\hat{T}_1$ and $\hat{T}_2$ indicate the solidus and liquidus temperatures, respectively ($\hat{T}_1 < \hat{T}_2$). The thermophysical properties in the mushy zone are assumed to be constant as [17]

$$\alpha_2 = \frac{k_2}{\rho_2 c_2}, \quad k_2 = \frac{k_1 + k_3}{2},$$
$$c_2 = \frac{c_1 + c_3}{2} + \frac{\hat{f}_1 \Delta h^*}{\hat{T}_2 - \hat{T}_1} \tag{32}$$

where c_2 is an effective specific heat into which the linear release of latent heat is absorbed. Owing to the use of these simplified relations, exact closed-form solutions can be obtained as in refs. [15–17]. (However, the solid fraction used in refs. [15, 16] varies linearly with distance instead of temperature.) Both planar and cylindrical geometries are considered as follows. The initial and boundary conditions are

$$\hat{x}_1 = \hat{x}_2 = 0 \quad \text{at} \quad t = 0$$
$$T_3 = \hat{T}_3 \quad \text{at} \quad t = 0 \quad \text{and} \quad x = \infty$$
$$\left.\begin{aligned} &\text{if} \quad n = 0: \quad T_1 = \hat{T}_0 \\ &\text{if} \quad n = 1: \quad \lim_{x \to 0} 2\pi x k_1 \frac{\partial T_1}{\partial x} = Q \end{aligned}\right\} \quad \text{at} \quad x = 0 \tag{33}$$

where Q is a heat sink at the origin [17]. The interface conditions are

$$T_i = T_{i+1} = \hat{T}_i,$$
$$k_i \frac{\partial T_i}{\partial x} - k_{i+1} \frac{\partial T_{i+1}}{\partial x} = \rho_i (h_{i+1} - h_i) \frac{\mathrm{d}\hat{x}_i}{\mathrm{d}t} \tag{34}$$

where $i = 1, 2$. The latent heats at both interfaces are specified as

$$h_2 - h_1 = \Delta h^*(1 - \hat{f}_1) \quad \text{at} \quad T = \hat{T}_1$$
$$h_3 - h_2 = 0 \quad \text{at} \quad T = \hat{T}_2. \tag{35}$$

Then, it can be easily shown that, in the case of $c_1 \neq c_3$, the above system of equations is thermodynamically consistent only when h_2 and T^* are chosen such that

$$h_2 = c_2(T_2 - \hat{T}_2) + \Delta h^* + c_3(\hat{T}_2 - T^*),$$
$$T^* = \frac{\hat{T}_1 + \hat{T}_2}{2}. \tag{36}$$

However, this point was not clearly mentioned in ref. [17]. Note that if $\hat{f}_1 = 1$ the enthalpy discontinuity no longer exists throughout the system. In the case of planar geometry, analytical solutions are obtained in terms of a similarity variable $\eta = x(4\alpha_2 t)^{-1/2}$ as follows:

$$\hat{x}_1(t) = 2\lambda_1\sqrt{(\alpha_2 t)}, \quad \hat{x}_2(t) = 2\lambda_2\sqrt{(\alpha_2 t)}$$
$$\frac{T_1 - \hat{T}_0}{\hat{T}_1 - \hat{T}_0} = \frac{\operatorname{erf}(\beta_1\eta)}{\operatorname{erf}(\beta_1\lambda_1)}$$
$$\frac{T_2 - \hat{T}_1}{\hat{T}_2 - \hat{T}_1} = \frac{\operatorname{erf}(\eta) - \operatorname{erf}(\lambda_1)}{\operatorname{erf}(\lambda_2) - \operatorname{erf}(\lambda_1)}$$
$$\frac{T_3 - \hat{T}_3}{\hat{T}_2 - \hat{T}_3} = \frac{\operatorname{erfc}(\beta_2\eta)}{\operatorname{erfc}(\beta_2\lambda_2)}$$
$$\beta_1 = \sqrt{\left(\frac{\alpha_2}{\alpha_1}\right)}, \quad \beta_2 = \sqrt{\left(\frac{\alpha_2}{\alpha_3}\right)}. \tag{37}$$

In the above, the similarity constants λ_1 and λ_2 are obtained from

$$\frac{c_3(\hat{T}_3 - \hat{T}_2)}{H(\beta_2\lambda_2)} = \frac{c_2(\hat{T}_2 - \hat{T}_1)}{G(\lambda_2) - \lambda_{12}G(\lambda_1)}$$
$$\frac{c_1(\hat{T}_1 - \hat{T}_0)}{G(\beta_1\lambda_1)} - \frac{c_3(\hat{T}_3 - \hat{T}_2)\lambda_{12}}{H(\beta_2\lambda_2)} = \Delta h^*(1 - \hat{f}_1) \tag{38}$$

where $\lambda_{12} = (\lambda_2/\lambda_1)\exp(\lambda_2^2 - \lambda_1^2)$ and the functions $G(x)$ and $H(x)$ are defined in equation (24). The above analytical solutions were derived from those in ref. [16] by modifying the expression for the solid fraction. Numerical solutions are obtained for various values of $\hat{f}_1$ with other parameters given below

$$Ste = 0.435, \quad c_3 = 1.20c_1, \quad k_3 = 0.92k_1$$
$$\hat{\theta}_0 = 0.870, \quad \hat{\theta}_1 = 0.946, \quad \hat{\theta}_2 = 1.054, \quad \hat{\theta}_3 = 1.062. \tag{39}$$

Table 3. Analytical solutions for λ_1 and λ_2 from equations (38)

$\hat{f}_1$	λ_1	λ_2
0.0	0.2238	1.3550
0.3	0.3041	1.5661
0.6	0.3586	1.6820
1.0	0.4129	1.7835

The exact solutions for λ_1 and λ_2 corresponding to the above case are listed in Table 3. Note that if $\hat{f}_1 = 0$ the latent heat is released at the solidus front only. Numerical solutions are obtained by employing the power-law scheme and by using $M_1 = 10$, $M_2 = 20$ and $M_3 = 100$. From the nature of the problem, $\omega'_0 = 0$ and $\omega'_3 = \omega'_2$ are chosen so that the correction equation (17) yields two linear equations for two unknowns ω'_1 and ω'_2. Converged solutions are obtained typically within five iterations. Numerical results for λ_1 and λ_2 are found to agree to within 0.4% with the corresponding analytical solutions during the interval $10^{-4} < \delta_1/l^* < 10^5$.

In the case of cylindrical geometry, exact solutions are found in ref. [17] where a system made of aluminum–copper alloy containing 5% copper [15] is considered to illustrate analytical results. The present numerical method is applied to this problem with $M_1 = 50$, $M_2 = 200$ and $M_3 = 200$. The parameters used in the computation can be found in ref. [17]. Computation is performed without initializing from the exact solutions, and, therefore, a large number of iterations (up to 300) were required at small times. However, numerical solutions converge within three iterations during the interval $10^{-3} < \delta_1/l^* < 10^5$. This reduction in the number of iterations is due to the asymptotic behavior in the solution discussed previously. The values of λ_1 and λ_2, as defined in equation (37), are listed in Table 4 where the present numerical solutions and the exact solutions from ref. [17] are compared. A disagreement between two results at a small value of Q can be improved (to within 1%) by increasing the number of grid points.

3.3. *Model III*

This model assumes that the specific enthalpy and the thermal properties in the mushy zone (designated by no subscript) are weighted with respect to the local solid fraction [32] as

Table 4. Analytical solutions for similarity constants λ_1 and λ_2 from ref. [17] and the present numerical results (shown inside parentheses)

Q [W m^{-1}]	$\beta_1\lambda_1$	λ_2
20000	0.00102 (0.00121)	0.8367 (0.8366)
30000	0.00712 (0.00717)	0.9777 (0.9777)
40000	0.01879 (0.01883)	1.0724 (1.0724)
50000	0.03377 (0.03384)	1.1433 (1.1435)
70000	0.06694 (0.06716)	1.2476 (1.2482)

$$h = fh_S + (1-f)h_L$$
$$c = fc_S + (1-f)c_L$$
$$k = fk_S + (1-f)k_L \qquad (40)$$

where $\rho = \rho_S = \rho_L$ is assumed, and h_S and h_L are determined from equation (1). The local solid fraction, which is commonly related to the liquidus curve of the phase diagram [18, 19], is expressed as an explicit function of the temperature. In particular, a planar geometry is considered; thus the heat diffusion equation in the mushy phase is written as

$$\frac{\partial}{\partial t}(\rho h) = \frac{\partial}{\partial x}\left(\frac{k}{c_S}\frac{\partial h}{\partial x}\right) + \frac{\partial}{\partial x}\left(\frac{k}{c_S}\frac{\partial \psi}{\partial x}\right) \qquad (41)$$

where $\psi = h_S - h$ [23]. The combined flux terms (including the interfacial fluxes) are upwinded and a linear profile for ψ is used in deriving discretization equations. The motivation for this special treatment is explained in ref. [24]. However, the solid and liquid phases are treated by employing the power-law scheme as in other models. Due to the nonlinearity, the numerical solution of equation (41) requires iterations. If the temperature field in the mushy zone is known at the previous iteration, all other quantities (such as f, h_S and h_L, etc.) are then evaluated from this known temperature field. Since h is the dependent variable in the discretization equation [24], a new value of h (say h^N) is obtained as the current solution. Then, the temperature is updated using the value of h^N as follows. Expanding h^N in terms of f' and T' and neglecting higher-order terms gives

$$h^N = h + \left(\frac{\partial h}{\partial T}\right)T' + \left(\frac{\partial h}{\partial f}\right)f'$$

or

$$h^N = h + \left\{c + (h_S - h_L)\left(\frac{\mathrm{d}f}{\mathrm{d}T}\right)\right\}T' \qquad (42)$$

from which the updated temperature is determined as

$$T^N \equiv T + T' = T + \frac{h^N - h}{c + (h_S - h_L)(\mathrm{d}f/\mathrm{d}T)}. \qquad (43)$$

Iteration continues with the updated temperature field until converged solutions are obtained.

As an illustrative example, the system considered in Model II is selected due to the close relationship between this model and Model II. Therefore, the initial and boundary conditions are given in equations (33) and (34), and a reference temperature T^* is given in equation (36). Also, the parameters in equation (39) and the f–T relation in equation (31) are used; however, the present numerical method can accommodate a general f–T relation. When the interfacial fluxes into and away from the mushy phase are evaluated, including the last term of equation (41), the correction equation (17) is still applicable to this problem and gives two linear equations for ω'_1 and ω'_2. Computation is carried out with $M_1 = 20$, $M_2 = 50$

and $M_3 = 100$. Similarity constants λ_1 and λ_2 are evaluated from the numerical solutions for the positions of the solidus and liquidus fronts such that

$$\lambda_1 = \frac{\hat{x}_1(t)}{2\sqrt{(\alpha^* t)}}, \quad \lambda_2 = \frac{\hat{x}_2(t)}{2\sqrt{(\alpha^* t)}} \tag{44}$$

where α^* is determined from equation (32), i.e. $\alpha^* = \alpha_2$, rather than from equation (40). As was discussed, the transformed coordinate plays the role of similarity variable and thus eliminates the dependence of the temperature distribution on time. This is clearly shown in Fig. 4 where the temperature profiles for the case of $\hat{f}_1 = 1$ are plotted with respect to the transformed coordinate. The solid lines represent the numerical results, while the points are the exact solutions that are obtained from equation (37) with the values of λ_1 and λ_2 evaluated from equation (44). In Fig. 4, a single curve within each phase is in reality the superposition of the numerical solutions in the range of $10^{-4} < \delta_1/l^* < 10$. Agreement with exact solutions is rather good (closed-form solutions are possible only in the solid and liquid phases). The temperature profiles in the mushy phase for different values of $\hat{f}_1$ are shown in Fig. 5 where the values of λ_1 and λ_2 are also listed. Converged solutions are obtained within ten iterations during the initial transient period and thereafter within four iterations. Figure 5 shows that, as the value of $\hat{f}_1$ increases, the temperature profiles are shifted towards the solidus front. This can be explained from the following argument, which is similar to that leading to equation (28). By manipulating equations (6) and (44), the Peclet number at a given control-volume surface located within the mushy zone can be expressed as

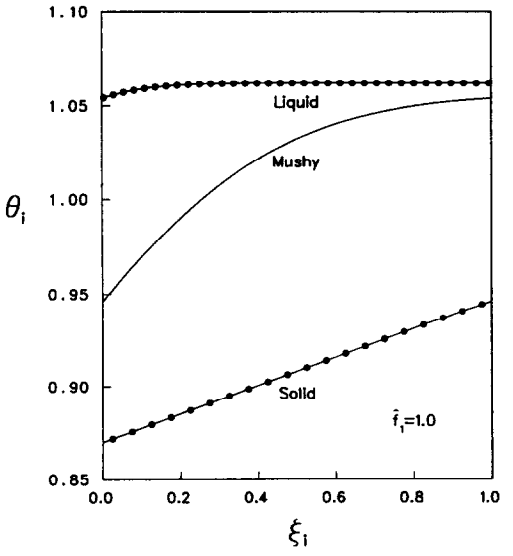

FIG. 4. Temperature distribution in the solid, mushy and liquid phases for the case of $\hat{f}_1 = 1$: numerical solutions (solid lines) and exact solutions (circles).

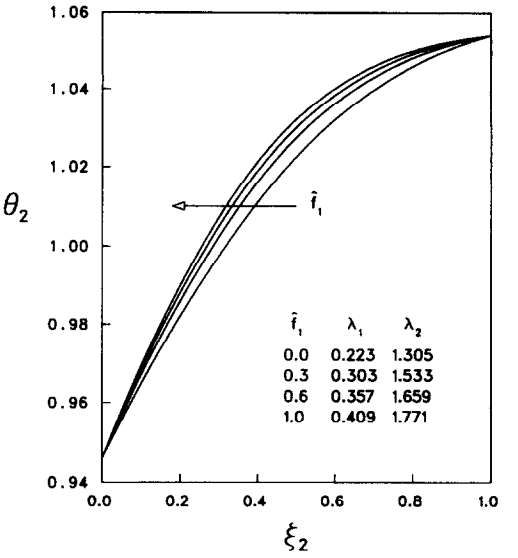

FIG. 5. Temperature distribution in the mushy phase for various values of $\hat{f}_1$.

$$|P| \sim \frac{\rho(\partial x/\partial t)}{\Gamma/[\delta_2(\Delta\xi)]} \sim \left\{\frac{2\rho\alpha^*}{\Gamma/(\Delta\xi)}\right\} \times \left(\xi_2 + \frac{\lambda_1}{\lambda_2 - \lambda_1}\right)(\lambda_2 - \lambda_1)^2. \tag{45}$$

An examination of the above equation using the values of λ_1 and λ_2 from Fig. 5 shows that the Peclet number increases with an increase in $\hat{f}_1$. Therefore, as the value of $\hat{f}_1$ increases, a higher upwinding occurs due to an increased Peclet number. Also, since the direction of pseudo-convection is towards the solidus front, the temperature profile is shifted towards the solidus front.

In refs. [18, 19], the wall temperature is set above the solidus temperature. Thus a single moving interface separating the mushy and liquid phases (i.e. liquidus front) is considered. Their numerical solutions are based on the use of ordinary differential equations expressed in terms of a similarity variable. These approaches require the analytical solutions for the liquid phase and, therefore, are of a limited applicability to semi-infinite domain problems. Note that the present numerical method has eliminated such a limitation and is also applicable to finite-domain problems.

4. SUMMARY

The conservative transformed equation recently proposed by the authors is utilized to solve diffusion-controlled solidification of binary alloys. The numerical method suggested here is suitable to treat a certain class of diffusion models based on the assumptions of

macroscopically planar interface and local thermodynamic equilibrium.

In the literature, analytical solutions are normally found for unbounded-domain problems by converting partial differential equations into ordinary differential equations in terms of a similarity variable. Analytical solutions are sometimes combined with numerical solutions based on conventional methods such as the Runge–Kutta integration. In the present numerical method, the partial differential form is retained in the transformed coordinate, which often plays the role of a similarity variable. As a result, an analogous pattern is found between the numerical and the analytical solutions. However, the present numerical method has a capability to treat finite-domain problems as well, and its formulation is based on the conservation principles and thus is consistent with well-established solution methods in treating fixed-boundary problems. Furthermore, when compared with the existing numerical methods based on multi-domain approaches, the present method employs a remarkably different solution procedure. As such, the temperature and position corrections, similar to the pressure-correction widely used in single-phase convection/diffusion problems, are introduced to overcome the difficulties associated with unknown location of phase interface and unknown interface temperature. The correction equations are derived from the conservation of the interfacial fluxes and are solved simultaneously to update the intermediate solutions during iterations. Therefore, the present numerical method is characterized by a fully-implicit treatment of the field equations and the interface conditions, and, consequently, the conservation principles are obeyed within a preselected tolerance.

The present numerical method is tested against several diffusion models for which analytical solutions are at least partially available. In the case of no mushy-zone models, both the temperature and concentration fields are treated by employing proper renormalization of the length scales to resolve steep concentration gradients near the phase interface. Solutions to the mushy-zone models, in which the growth of the mushy zone is controlled by heat diffusion, are also studied. In addition, an assumption that is thermodynamically inconsistent but found in some of the previous studies is addressed and examined quantitatively. A novel technique developed in this study enables the numerical solution at each time step to converge within a small number of iterations. Also, numerical solutions agree with the available analytical solutions to within reasonable accuracies. The present numerical method can potentially treat the two-dimensional cases of the models considered here.

REFERENCES

1. C.-J. Kim and M. Kaviany, A numerical method for phase-change problems, *Int. J. Heat Mass Transfer* **33,** 2721–2734 (1990).
2. C.-J. Kim and M. Kaviany, A numerical method for phase-change problems with convection and diffusion, *Int. J. Heat Mass Transfer* **35,** 457–467 (1992).
3. M. C. Flemings, *Solidification Processing*. McGraw-Hill, New York (1974).
4. R. Viskanta, Mathematical modeling of transport processes during solidification of binary systems, *JSME Int. J. Series II* **33,** 409–423 (1990).
5. C. Wagner, Theoretical analysis of diffusion of solutes during the solidification of alloys, *Trans. AIME J. Metals* 154–160 (1954).
6. L. I. Rubinstein, *The Stefan Problem*. English translation published by the American Mathematical Society, Providence, Rhode Island (1971).
7. T. Tsubaki and B. A. Boley, One-dimensional solidification of binary mixtures, *Mech. Res. Commun.* **4,** 115–122 (1977).
8. B. A. Boley, Time-dependent solidification of binary mixtures, *Int. J. Heat Mass Transfer* **21,** 821–824 (1978).
9. S. C. Gupta, Numerical and analytical solutions of one-dimensional freezing of dilute binary alloys with coupled heat and mass transfer, *Int. J. Heat Mass Transfer* **33,** 593–602 (1990).
10. G. H. Meyer, A numerical method for the solidification of a binary alloy, *Int. J. Heat Mass Transfer* **24,** 778–781 (1981).
11. K. Wollhöver, Ch. Körber, M. W. Scheiwe and U. Hartmann, Unidirectional freezing of binary aqueous solutions: an analysis of transient diffusion of heat and mass, *Int. J. Heat Mass Transfer* **28,** 761–769 (1985).
12. J. J. Derby and R. A. Brown, A fully implicit method for simulation of the one-dimensional solidification of a binary alloy, *Chem. Engng Sci.* **41,** 37–46 (1986).
13. R. L. Levin, The freezing of finite domain aqueous solutions: solute redistribution, *Int. J. Heat Mass Transfer* **24,** 1443–1455 (1981).
14. D. G. Wilson, A. D. Solomon and V. Alexiades, A shortcoming of the explicit solution for the binary alloy solidification problem, *Lett. Heat Mass Transfer* **9,** 421–428 (1982).
15. R. H. Tien and G. E. Geiger, A heat-transfer analysis of the solidification of a binary eutectic system, *Trans. ASME J. Heat Transfer* 230–234 (1967).
16. S. H. Cho and J. E. Sunderland, Heat-conduction problems with melting and freezing, *Trans. ASME J. Heat Transfer* 421–426 (1969).
17. M. N. Özişik and J. C. Uzzell, Jr., Exact solution for freezing in cylindrical symmetry with extended freezing temperature range, *J. Heat Transfer* **101,** 331–334 (1979).
18. L. J. Fang, F. B. Cheung, J. H. Linehan and D. R. Pedersen, Selective freezing of a dilute salt solution on a cold ice surface, *J. Heat Transfer* **106,** 385–393 (1984).
19. S. L. Braga and R. Viskanta, Solidification of a binary solution on a cold isothermal surface, *Int. J. Heat Mass Transfer* **33,** 745–754 (1990).
20. M. G. Worster, Solidification of an alloy from a cooled boundary, *J. Fluid Mech.* **167,** 481–501 (1986).
21. R. C. Kerr, A. W. Woods, M. G. Worster and H. E. Huppert, Solidification of an alloy cooled from above: Part 3. Compositional stratification within the solid, *J. Fluid Mech.* **218,** 337 354 (1990).
22. R. E. Sonntag and G. Van Wylen, *Introduction to Thermodynamics Classical & Statistical*. Wiley, New York (1971).
23. W. D. Bennon and F. P. Incropera, A continuum model for momentum, heat and species transport in binary solid–liquid phase change systems, *Int. J. Heat Mass Transfer* **30,** 2161–2187 (1987).
24. W. D. Bennon and F. P. Incropera, Numerical analysis of binary solid–liquid phase change using a continuum model, *Numer. Heat Transfer* **13,** 277–296 (1988).
25. C. Prakash, Two-phase model for binary solid–liquid phase change, *Numer. Heat Transfer* **18B,** 131–167 (1990).

26. S. V. Patankar, *Numerical Heat Transfer and Fluid Flow*. Hemisphere, Washington, DC (1980).
27. T. P. Battle and R. D. Pehlke, Mathematical modeling of microsegregation in binary metallic alloys, *Met. Trans. B* **21B**, 357–375 (1990).
28. E. M. Sparrow, S. Ramadhyani and S. V. Patankar, Effect of subcooling on cylindrical melting, *J. Heat Transfer* **100**, 395–402 (1978).
29. M. N. Özişik, *Heat Conduction*. Wiley, New York (1980).
30. J. Crank and R. S. Gupta, Isotherm migration method in two dimensions, *Int. J. Heat Mass Transfer* **18**, 1101–1107 (1975).
31. J. Crank and A. B. Crowley, Isotherm migration along orthogonal flow lines in two dimensions, *Int. J. Heat Mass Transfer* **21**, 393–398 (1978).
32. G. K. Batchelor, Transport properties of two-phase materials with random structure, *Ann. Rev. Fluid Mech.* **6**, 227–255 (1974).

UNE METHODE ENTIEREMENT IMPLICITE POUR LA SOLIDIFICATION CONTROLEE PAR LA DIFFUSION DANS DES ALLIAGES BINAIRES

Résumé—Une méthode numérique développée récemment pour des problèmes de changement de phase d'un composant unique est étendue au traitement de modèles de solidification contrôlée par la diffusion pour des alliages binaires. Les modèles multi-domaine soulèvent une difficulté spéciale associée à la position inconnue de l'interface et à la température de transition de phase. Cette difficulté est efficacement traitée ici en définissant des corrections semblables à celles utilisées dans les problèmes de convection monophasique. Les équations et les conditions interfaciales sont traitées de façon complètement implicite à l'aide des équations de correction qui sont développées à partir de la conservation des flux interfaciaux. Comme vérification, plusieurs modèles de diffusion conduisant à des solutions analytiques sont considérés. Les solutions numériques s'accordent avec les solutions analytiques disponibles. L'hypothèse très courante d'une chaleur latente constante est trouvée être thermodynamiquement inconsistante dans certaines conditions et elle est clarifiée et corrigée. Une procédure d'itération unique, suggérée dans cette étude, est remarquablement efficace et elle conduit à une convergence rapide.

EIN VOLLSTÄNDIG IMPLIZITES VERFAHREN FÜR DIE DIFFUSIONSKONTROLLIERTE ERSTARRUNG BINÄRER LEGIERUNGEN

Zusammenfassung—Ein kürzlich entwickeltes numerisches Verfahren für Phasenwechselprobleme mit einer Komponente wird erweitert, um vorhandene Mehrzonen-Modelle für die diffusionskontrollierte Erstarrung binärer Legierungen behandeln zu können. Die Mehrzonenmodelle rufen im Zusammenhang mit der unbekannten Lage der Phasengrenzfläche und der Phasenübergangstemperatur spezielle Schwierigkeiten hervor. Solch eine Schwierigkeit wird hier dadurch wirksam beseitigt, daß Korrekturen definiert werden, ähnlich denen, die bei einphasigen Konvektionsproblemen gebräuchlich sind. Die Feldgleichungen und die Bedingungen an der Phasengrenzfläche werden durch die Temperaturgleichungen implizit behandelt, welche sich aus den Stromdichten an der Phasengrenze ergeben. Zusätzlich wird beim Auftreten einer großen Abweichung zwischen thermisch- und konzentrationsbedingter Stoffdiffusion eine erneute Normierung der Längenskalen empfohlen, um die räumliche Auflösung sowohl des Temperatur- als auch des Konzentrationsfeldes zu verbessern. Als Verifikation werden mehrere Diffusionsmodelle betrachtet, für die auch analytische Lösungen vorliegen. Die Übereinstimmung ist gut. Es wird außerdem herausgefunden, daß die weithin benutzte Annahme konstanter latenter Wärme unter bestimmten Bedingungen thermodynamisch inkonsistent ist. Dieser Punkt wird geklärt und korrigiert. Ein eindeutiges Iterationsverfahren, das in der vorliegenden Untersuchung vorgeschlagen wird, hat sich als bemerkenswert wirksam herausgestellt und führt zu schneller Konvergenz.

НЕЯВНЫЙ МЕТОД РАСЧЕТА КОНТРОЛИРУЕМОГО ДИФФУЗИЕЙ ЗАТВЕРДЕВАНИЯ БИНАРНЫХ СПЛАВОВ

Аннотация—Недавно раработанный численный метод решения задач однокомпонентного фазового перехода распространяется на исследование некоторых многодоменных моделей для контролируемого диффузией процесса затвердевания бинарных сплавов. Использование многодоменных моделей связано с трудностями, обусловленными отсутствием данных о расположении границы раздела и температуре фазового перехода. Это затруднение эффективно устраняется посредством определения поправок, аналогичных встречающимся в конвективных задачах однофазных систем. Уравнения и условия на границе раздела формулируются в неявной форме, исходя из уравнения сохранения потоков на границе. Кроме того, при больших расхождениях между значениями коэффициентов температуропроводности и массопроводности растворенного вещества предполагается, что перенормировка масштабов длины повышает пространственное разрешение температурных и концентр ационных полей. Для проверки рассматриваются несколько моделей диффузии, допускающих аналитические решения. При этом численные решения хорошо согласуются с имеющимися аналитическими. Разъясняется и корректируется широко используемое предположение о постоянстве величины скрытой теплоты, которое, как показано, в определенных условиях становится неправомерным с точки зрения термодинамики. Предложенный оригинальный итерационный метод является весьма эффективным и приводит к быстрой сходимости.